Early Metabolic Disruption and Predictive Biomarkers of Delayed-Cerebral Ischemia in Aneurysmal Subarachnoid Hemorrhage

Karim Chikh, David Tonon, Thibaut Triglia, David Lagier, Anouk Buisson, Marie-Christine Alessi, Catherine Defoort, Sherazade Benatia, Lionel J Velly, Nicolas Bruder, et al.

Journal of proteome research

pubs.acs.org/jpr

Article

Early Metabolic Disruption and Predictive Biomarkers of Delayed-Cerebral Ischemia in Aneurysmal Subarachnoid Hemorrhage

Karim Chikh, David Tonon, Thibaut Triglia, David Lagier, Anouk Buisson, Marie-Christine Alessi, Catherine Defoort, Sherazade Benatia, Lionel J. Velly, Nicolas Bruder, and Jean-Charles Martin*

Cite This: *J. Proteome Res.* 2024, 23, 316−328

Read Online

ACCESS | Metrics & More | Article Recommendations | Supporting Information

ABSTRACT: Delayed cerebral ischemia (DCI) following aneurysmal subarachnoid hemorrhage (aSAH) is a major cause of complications and death. Here, we set out to identify high-performance predictive biomarkers of DCI and its underlying metabolic disruptions using metabolomics and lipidomics approaches. This single-center prospective observational study enrolled 61 consecutive patients with severe aSAH; among them, 22 experienced a DCI. Nine patients without aSAH were included as validation controls. Blood and cerebrospinal fluid (CSF) were sampled within the first 24 h after admission. We identified a panel of 20 metabolites that, together, showed high predictive performance for DCI. This panel of metabolites included lactate, cotinine, salicylate, 6 phosphatidylcholines, and 4 sphingomyelins. The interplay of the metabolome and the lipidome found between CSF and plasma in our patients underscores that aSAH and its associated DCI complications can extend beyond cerebral implications, with a peripheral dimension as well. As an illustration, early biological disruptions that might explain the subsequent DCI found systemic hypoxia driven mainly by higher blood lactate, arginine, and proline metabolism likely associated with vascular NO and disrupted ceramide/sphingolipid metabolism. We conclude that targeting early peripheral hypoxia preceding DCI could provide an interesting strategy for the prevention of vascular dysfunction.

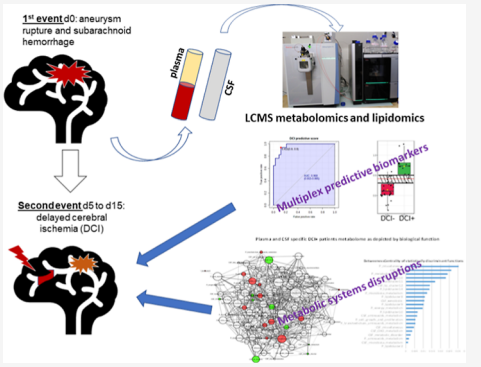

KEYWORDS: *delayed cerebral ischemia, aneurysmal subarachnoid hemorrhage, vasospasm, metabolomics, lipidomics*

INTRODUCTION

Delayed cerebral ischemia (DCI) occurs in about 30% of patients with aneurysmal subarachnoid hemorrhage (aSAH) within the first 2 weeks after hemorrhage.[1] DCI is responsible for increased morbidity and mortality.[2] It is crucial to identify patients at risk of developing DCI after aSAH in order to develop targeted therapies for treating or preventing this potentially life-threatening complication. However, there is still no established biomarker for predicting DCI. Furthermore, there is a broader need to more clearly establish the early biological disruptions that ultimately lead to DCI, as only hypotheses have been put forward. DCI was long thought to be caused by cerebral vasospasm, but recent studies support the notion that it is a multifactorial pathophysiology that includes cerebral vascular dysregulation, microthrombosis, cortical spreading depolarization, and neuroinflammation.[3]

Metabolomics and its subfield lipidomics are powerful tools for identifying putative biomarkers in various different contexts, from disease diagnostics[4] and disease risk analysis[5,6] to the prediction of therapeutic response.[7] Moreover, changes in the metabolome provide a molecular snapshot of cellular activity and thus provide important clues to understanding functional changes in the metabolic pathways that drive disease risk.

Modifications of some metabolites and lipid levels have been reported in the context of DCI or vasospasm associated with aSAH. Elevated CSF levels of ceramides,[8] arachidonic acid, linoleic acid, and palmitic acid,[9] elevated lactate/pyruvate ratio[10] and taurine in cerebral microdialysis samples,[11] high blood lactate levels and glucose levels,[12] and elevated plasma taurine levels[13] have all been reported in aSAH patients who later develop cerebral vasospasm and/or DCI. Nevertheless, there are no consensual biomarkers accepted for routine use in clinical practice.[14]

In a previous paper, we reported an early increase in CSF MMP-9 concentrations in patients who later developed DCI.[15] Here, we carried out both LC−MS/MS-based plasma and CSF metabolomic profiling and total gas-chromatography fatty acid analysis in our cohort of patients presenting aSAH with and without subsequent DCI. Our objectives were to identify

Received: September 7, 2023
Revised: November 27, 2023
Accepted: December 13, 2023
Published: December 27, 2023

predictive biomarkers of DCI and to decipher the early underlying metabolic pathway disruptions leading to DCI.

METHODS

Study Population and Prospective Study Setting

The study was designed and conducted following the Strengthening the Reporting of Observational Studies in Epidemiology guidelines.[16] Ethical approval for this study (N8 2013-1316) was provided by the institutional review board of the Assistance Public-Hôpitaux de Marseille, France (Chairperson: Professor Y. Jammes) on May 16, 2013. After obtaining written informed consent from the next of kin, we enrolled 61 consecutive patients with spontaneous aSAH who met the inclusion criteria. To be eligible for inclusion, patients had to be over 18 years old and admitted to the NCCU of La Timone University Hospital (Marseille) within 24 h postbleeding, and their conditions had to require clinically indicated external ventricular drainage. Patients were excluded if pregnant, if they had vasospasm on the first diagnostic angiogram, or if their condition was so severe that they were unlikely to survive more than 48 h. Patient details were collected, including age, gender, and individual scores on the Simplified Acute Physiology Score II disease severity classification system, the World Federation of Neurological Surgeons (WFNS) grading system, and the Hunt and Hess score, as described in Triglia et al.[15] Radiographic characteristics of the initial hemorrhage were identified, including localization of the aneurysm, modified Fisher grade, and volume of the intraventricular hemorrhage (IVH) evaluated using the IVH score, as explained in Triglia et al.[15] Radiographic grading-scale scores were determined by two authors (L.V. and D.L.) who were blinded to the clinical outcome of the patients studied. In addition, we collected data on duration of mechanical ventilation and external ventricular drainage placement, length of stay in the NCCU, modified Rankin Scale score, and Glasgow Outcome Scale extended at 1 month.[15] All patients were followed with transcranial Doppler sonography (TCD; Philips CX50 with a S3-1 transducer, Philips Healthcare, Suresnes, France) and received continuous intravenous nimodipine. Acceleration of TCD mean blood flow velocity above 120 cm s^{-1} in the middle or anterior cerebral artery or daily change in mean TCD velocities greater than 50 cm s^{-1} was suggestive of cerebral vasospasm. DCI was defined, based on the latest recommendations,[17] as follows: a development of focal neurological signs; a drop of at least 2 points on the Glasgow Coma Scale that lasts for at least 1 h and is associated with angiographic cerebral vasospasm, detected either with computed tomography (CT) angiography or digital subtraction angiography; or a new cerebral infarction detected by CT, either within 6 weeks after aSAH or before discharge, after first ruling out a procedure-related infarction. Patients without aSAH admitted to the NCCU for other neurological disorders (see Table S1) were included as control patients (n = 9). Blood and CSF were sampled in the first 24 h post-aSAH. CSF samples were collected from the external ventricular drain into anticoagulant-free sterile tubes. Blood samples were collected in sterile vacutainer citrate tubes. Samples were centrifuged for 10 min at 2500g at 4 °C and then immediately transferred to cryotubes and stored at −80 °C until analysis.

Method for the Metabolomics Analysis

Preparation of Dried Extracts and the LC−MS/MS Method. For metabolomics analysis, 100 μL of CSF or plasma samples was protein-precipitated with 400 μL of cold methanol (−20 °C). All the dried polar extracts of both CSF and plasma were first reconstituted with 125 μL of acetonitrile/water (90:10; v/v). The samples were separated using an Ultimate 3000 ultraperformance liquid chromatography (UPLC) (Thermo Scientific) coupled to a Q-Exactive Plus quadrupole-orbitrap hybrid high-resolution mass spectrometer (HRMS) equipped with a heated-electrospray ionization source (H-ESI II). Chromatographic separation was performed on a binary solvent system using a reverse-phase C18 column (Hypersil Gold, Thermo Scientific, 100 mm × 2.1 mm, 1.9 μm) at 40 °C at a flow rate of 0.4 mL min^{-1} and a HILIC column (Merk, SeQuant ZIC-HILIC, 150 mm × 2.1 mm, 5 μm, 200 A) at 25 °C at a flow rate of 0.25 mL min-1. The injection volume for both columns was 5 μL. The mobile phase consisted of a combination of solvent A (0.1% formic acid in water, v/v) and solvent B (0.1% formic acid in acetonitrile, v/v). The following gradient conditions were used: 0 to 1 min, isocratic 100% A; 1 to 11 min, linear from 0 to 100% B; 11 to 13 min, isocratic 100% B; 13 to 14 min, linear from 100% to 0% B; and 14 to 16 min, isocratic 100% A. The separated molecules were analyzed in both positive and negative ionization modes in the same run. The mass spectra were collected using 35,000 full-width at half-maximum (fwhm) resolving power for the theoretical mass-to-charge ratio (m/z) of 200. Full-scan mass spectra were acquired in the 80−1000 m/z range. The ionization source parameters for positive and negative ion modes were as follows: capillary temperature 320 °C, spray voltage 3.5 kV, sheath gas 30 (arbitrary units), auxiliary gas 8 (arbitrary units), probe heater temperature 310 °C, and S-lens RF level set at 55 v. MS/MS experiments were performed using higher-energy collision-induced dissociation (HCD), and the normalized collision energy (NCE) applied was ramped from 10% to 40%. To ensure good repeatability of the analysis, a quality control sample (QC) was formed by pooling a small aliquot of each biological sample. The QC sample was analyzed intermittently (1 out of every 4 samples) for the duration of the analytical study to assess the variance observed in the data throughout the sample preparation, data acquisition, and data preprocessing steps.

The mobile phase for HILIC column separation consisted of a combination of solvent A (100% water, 16 mM ammonium formate) and solvent B (100% acetonitrile and 0.1% formic acid). The following gradient conditions were used: 0−2 min, isocratic 97% B; 2−10 min, linear from 97 to 70% B; 10 to 15 min, linear from 70 to 10% B; 15 to 17 min, isocratic 10% B; 17 to 18 min, linear from 10 to 97% B; and 18 to 22 min, isocratic 97% B. The separated molecules were analyzed in both positive and negative ionization modes in the same run. The mass acquisition parameters were the same as those used for the C18 column. The repeatability of the analysis was checked by analyzing the replicates of the QC sample.

Data Processing and Molecule Identification. After LC/MS acquisition, raw data files of the full scan—MS1 in both positive and negative modes—were converted into mzXML files. The data were processed using the R package XCMS (https://bioconductor.org/packages/release/bioc/html/xcms.html), as described in a previous paper,[18] to generate a data matrix of deconvoluted ions with m/z,

https://doi.org/10.1021/acs.jproteome.3c00575
J. Proteome Res. 2024, 23, 316−328

retention time, and intensity. For metabolomics analysis, the XCMS matrix was annotated using an internal database of more than 1300 reference compounds (based on exact mass and retention time and MS/MS spectra when detected).[18] For lipidomics analysis, the XCMS matrix was annotated using MS/MS data imported into LipidSearch 4.1 software (Thermo Fisher Scientific, San Jose, CA) and XCMS, as described in ref 19. The annotated metabolomics and lipidomics data sets were further processed by probabilistic quotient normalization to prevent sample-to-sample variation in the MS intensity response. All data sets were then combined with total fatty acid content in both plasma and CSF to obtain a single data matrix that served for further statistical analysis.

Methods for Lipidomics Analysis

Sample Extractions, LC−MS/MS Method, and Data Processing. Plasma and CSF samples were extracted, as described previously[18] (apolar extract). The dried extracts were then taken up in 120 μL of acetonitrile/water solution (1:1) and vortexed and centrifuged at 11,000g for 10 min at 4 °C. The samples were separated using an Ultimate 3000 UPLC (Thermo Scientific) coupled to a Q-Exactive Plus quadrupole-orbitrap hybrid HRMS equipped with a heated-electrospray ionization source (H-ESI II). Chromatographic separation was performed at a flow rate of 0.4 mL min^{-1} using an Accucore C18 column (Thermo Scientific, 150 × 2.1 mm, 2.6 μm) at 45 °C. The mobile phase consisted of a combination of solvent A (water/acetonitrile; 60:40 (v/v); 10 mM ammonium formate) and solvent B (isopropanol/acetonitrile 90:10 (v/v); 10 mM ammonium formate). The injection volume was 5 μL. The following gradient conditions were used: 0 to 4 min, linear from 35 to 60% B; 4 to 12 min, linear from 60 to 85% B; 12−21 min, linear from 85 to 100% B; 21 to 24 min, isocratic 100% B; at 24 min, dropped to 35% B; and from 24 to 28 min, isocratic 35% B. The separated molecules were analyzed in both positive and negative ionization modes in the same run. The mass spectra were collected using 35,000 full-width at half-maximum (fwhm) resolving power for the theoretical mass-to-charge ratio (m/z) of 200. Full-scan mass spectra were acquired in the 250−1200 m/z range. The ionization source parameters for positive and negative ion modes were as follows: capillary temperature 285 °C, spray voltage 3.5 kV, sheath gas 60 (arbitrary units), auxiliary gas 20 (arbitrary units), probe heater temperature 370 °C, and S-lens RF level set at 45 v. Except for MS/MS, experiments were performed using HCD, and the NCE applied was ramped from 10% to 40%. MS/MS acquisitions were performed intermittently throughout the analysis sequence at intervals of 10 samples. The purpose of MS/MS fragmentation is to generate fragments for each metabolite that can serve to determine in silico the structure of the lipid molecule and its identity using LipidSearch 4.1 software (Thermo Fisher Scientific, San Jose, CA). The data were processed using XCMS and LipidSearch, as described in ref 19.

Total Fatty Acid Quantification

Total plasma and CSF fatty acid compositions were measured using gas chromatography with a flame ionization detection system.[19] 250 μL of plasma and 1.9 mL of a stock methylation solution (1.8 mL of methanol and 100 μL of freshly prepared acetyl chloride) were combined in screw-capped glass tubes. The tubes were then capped, heated at 100 °C for 60 min, and left to cool to room temperature. Hexane (1 mL) was then added, and the tubes were vortexed for 30 s. The upper organic phase was collected with a Pasteur pipet. This extraction procedure was repeated, as described above, in order to optimize the extraction of fatty acid methyl esters. The combined hexane solutions were then evaporated under nitrogen to dryness, and the dry residue was dissolved in 100 μL of hexane, transferred to GC vials, and capped under nitrogen. Fast GC analyses were performed with a PerkinElmer Clarus 680 system on 0.5 μL of sample injected in the split mode by hydrogen flow at a rate of 10 mL/min. The column used was a BP × 70 capillary column of 10 m × 0.1 mm ID × 0.2 μm film thickness (SGE International Pty. Ltd., Australia). The temperature program was as follows: initial, 60 °C with a 0.5 min hold; ramp: 20 °C/min to 200, 7 °C/min to 225 °C with a 1 min hold, and then 160 °C/min to 250 °C with a 1 min hold. Instrumental conditions were as follows: carrier gas was H2 at a flow rate of 61.4 cm/s and a constant head pressure of 206.8 kPa; a flame ionization detector set at 280 °C; air and nitrogen makeup gas flow rates of 450 and 45 mL/min, respectively; a split ratio of 200:1; a sampling frequency of 50 Hz; and a 0.5 μL autosampler injection volume. The run-time for a single sample was 13.23 min, and the sample turnaround time was 16 min.

Statistical Analyses

Continuous variables were reported as the mean plus standard deviation. For univariate statistics, the data were transformed by Pareto scaling to obtain a Gaussian distribution across patients. Intergroup comparisons of means were performed using a t-test with adjustments for the false discovery rate.

For metabolomics data, features from both ionization modes for HILIC and RP data were combined into a single data set, while both ionization modes were combined for the lipid data. All data were mean-centered and divided by the standard deviation of each variable (autoscaling mode). Univariate statistical analysis, simple PLS-DA, random forest, hierarchical clustering, heatmapping, power calculation, ROC analysis, and correlation plotting were all performed using the online tool MetaboAnalyst 5.0. Partial correlations were calculated with the R package GeneNet, and network visualization was performed using Cytoscape. Hierarchical PLS-DA and multiplex biomarker score calculations were performed with a SIMCA 12 (Umetrics, Umea, Sweden). To minimize overfitting, models were validated by cross-validation analysis of variance (CV-ANOVA) (significance threshold ≤ 0.05) and by permutation tests (200 permutations). The biomarker identification process only used data from 50 patients, as CSF plus plasma data were not available for 11 patients. A DCI + score equation to predict the clinical status of each patient was calculated using the partial least-squares (PLS) algorithm combining all the individual discriminating variables, as described elsewhere.[6,18]

Discriminant metabolites in the PLS-DA analysis were determined from their variable importance in projection (VIP) values determined by the NIPALS algorithm. The significant threshold of VIP was calculated using a normal probability plot, indicating which VIP values of the corresponding metabolites deviated the most from the normal distribution due to treatment. A similar method was employed to select the PLS-DA VIP cutoff threshold for significant lipid species. Hierarchical-PLS-DA modeling was performed based on the contribution of separate orthogonal PLS-DAs calculated from all functional sets of metabolites, enabling us to generate a composite score value for each functional set. Multiblock PLS,

https://doi.org/10.1021/acs.jproteome.3c00575
J. Proteome Res. 2024, 23, 316−328

Table 1. Patient-Sample Characteristics

	all patients (n = 61 patients)	DCI− (n = 39 patients)	DCI+ (n = 22 patients)	unadjusted p value	adjusted P value (FDR)
Demographic variables, risk factors, and comorbidities					
men	28 (45.9%)	17 (43.6%)	11 (50%)	0.64	0.83
age, years	55.6 ± 12.4	58.2 ± 11.8	51.0 ± 12.4	**0.03***	0.23
diabetes mellitus	6 (9.8%)	5 (12.8%)	1 (4.5%)	0.31	0.65
dyslipidaemia	6 (9.8%)	4 (10.3%)	2 (9.1%)	0.89	0.89
smoking	22 (36.1%)	11 (28.2%)	11 (50%)	0.09	0.39
alcohol	12 (19.7%)	7 (17.9%)	5 (22.7%)	0.66	0.83
BMI	25.5 ± 5.3	26.3 ± 5.9	24.2 ± 4.0	0.79	0.85
hypertension	21 (34.4%)	15 (38.5%)	6 (27.3%)	0.39	0.65
dysthyroidism	7 (11.5%)	5 (12.8%)	2 (9.1%)	0.67	0.83
depression	9 (14.8%)	6 (15.4%)	3 (13.6%)	0.86	0.89
migraine	6 (9.8%)	2 (5.1%)	4 (18.2%)	0.10	0.39
Clinical presentation, complications and outcomes					
WNFS scale	3.7 ± 1.3	3.5 ± 1.4	3.9 ± 1.2	0.25	0.65
fischer grade	3.8 ± 0.5	3.7 ± 0.6	3.9 ± 0.4	0.39	0.65
vasospasm	20 (32.8%)	0 (0%)	20 (90.1%)	**2.6×10^{-27}**	**3.9×10^{-26}**
favorable GOSE	39 (63.9%)	27 (69.2%)	12 (54.5%)	0.29	0.65

or hierarchical PLS, enables the aggregation of the data into biological function blocks to ease data interpretation and a biological understanding of the implications of DCI on the system. The functional metabolic blocks were "weighted" to take into account the number of metabolites per block.[20] For lipid blocking, lipid species were grouped according to clusters calculated by hierarchical clustering analysis (Ward method). Lipid block score values were generated by Hierarchical-PLS-DA, as above. Scores from the Hierarchical-PLS-DA analysis were analyzed to determine the most significant biological functions related to clinical outcome using a t-test after adjustment for FDR ($P_{adj} \leq 0.05$), random forest, and PLS-DA analyses. The blocks selected by at least two statistical methods were retained (Figure S5) and were also graphed in a partial correlation network to assess the importance of each block (function) in the integrated system, as determined by the betweenness centrality topology coefficient of the network (calculated using the Cytoscape tool "NetworkAnalyser").

Pathway enrichment was performed using the enrichment tool bundled with MetaboAnalyst ((http://www.metaboanalyst.ca) for polar and semipolar metabolites and LION for lipids (http://www.lipidontology.com).

RESULTS

Clinical Features of the Studied Population

Among all of the patients with aSAH admitted to our NCCU between 2013 and 2016, 61 patients met the inclusion criteria. Of these 61 patients, 22 developed DCI (DCI+ group), whereas 39 did not (DCI− group). Patient-sample characteristics are reported in Table 1 and Figure S1. The only significant between-group difference in demographic variables was for patient age: DCI+ patients were significantly younger than DCI− patients. The DCI+ group tended to have more smokers and more cases of migraine. Vasospasm was identified in 90.1% of DCI+ patients but none in DCI− patients (p < 0.001).

Results are expressed as a number (%) or as the mean ± SD. DCI, delayed cerebral infarction; BMI, body mass index; WNFS, World Federation of Neurological Surgeons grading system scale; and GOSE, Glasgow Outcome Scale-Extended.* Student t-test p-values for patients with DCI (DCI+) vs those without DCI (DCI−) were considered significant at <0.05.

Values were transformed by Pareto scaling to obtain a Gaussian distribution across patients (see Figure S1).

Feature Detection in Metabolomics and Lipidomics Analysis and Fatty Acid Content

A total of 180 and 153 annotated metabolites and 166 and 290 annotated lipids were identified in CSF and plasma, respectively. In addition to metabolomics and lipidomics, 27 fatty acids were quantified in CSF and plasma by a targeted method. The overlap was 31.9% of common metabolites and 18.2% of common lipid species in the 2 biofluids. The fatty acids were similar in both CSF and plasma (Figure S2). A unique data matrix featuring 843 variables was built with all of these compounds and used for further statistical analyses. Missing values (4 in plasma and 16 in CSF) for fatty acids were replaced by an estimate based on Bayesian principal component analysis.

Biomarker Selection and Validation

As both CSF and plasma were not available for 6 and 5 patients, respectively, the biomarker identification process only used data from 50 patients of our cohort (33 DCI− and 17 DCI+). To select and validate a set of biomarkers, we applied an iterative workflow with randomly left-out patients in multiple predictive PLS-DA models.[6,18] PLS regression also allowed one to predict class assignments for unknown patients. A list of 20 metabolites was selected based on the most commonly shared variables found in 8 consecutively constructed PLS-DA training models in which four DCI− patients and two DCI+ patients were repeatedly and randomly left out. In each model, the variables were selected based on the shift in the PLS variable importance in projection score (VIP) from the normal distribution. The accuracy, goodness-of-fit R2, and goodness-of-prediction Q2 of the final PLS-DA model comprising all the individuals and based on these 20 selected metabolites were 0.89, 0.69, and 0.55, respectively (Figure 1a). All these 20 metabolites were significantly different between DCI− and DCI+ on a univariate t-test (FDR adjusted p-values < 0.05): 12 of these metabolites were relatively higher in abundance and 8 were relatively lower in abundance in DCI+ patients, and only 3 of them came from CSF (Figure 1b).

https://doi.org/10.1021/acs.jproteome.3c00575
J. Proteome Res. 2024, 23, 316−328

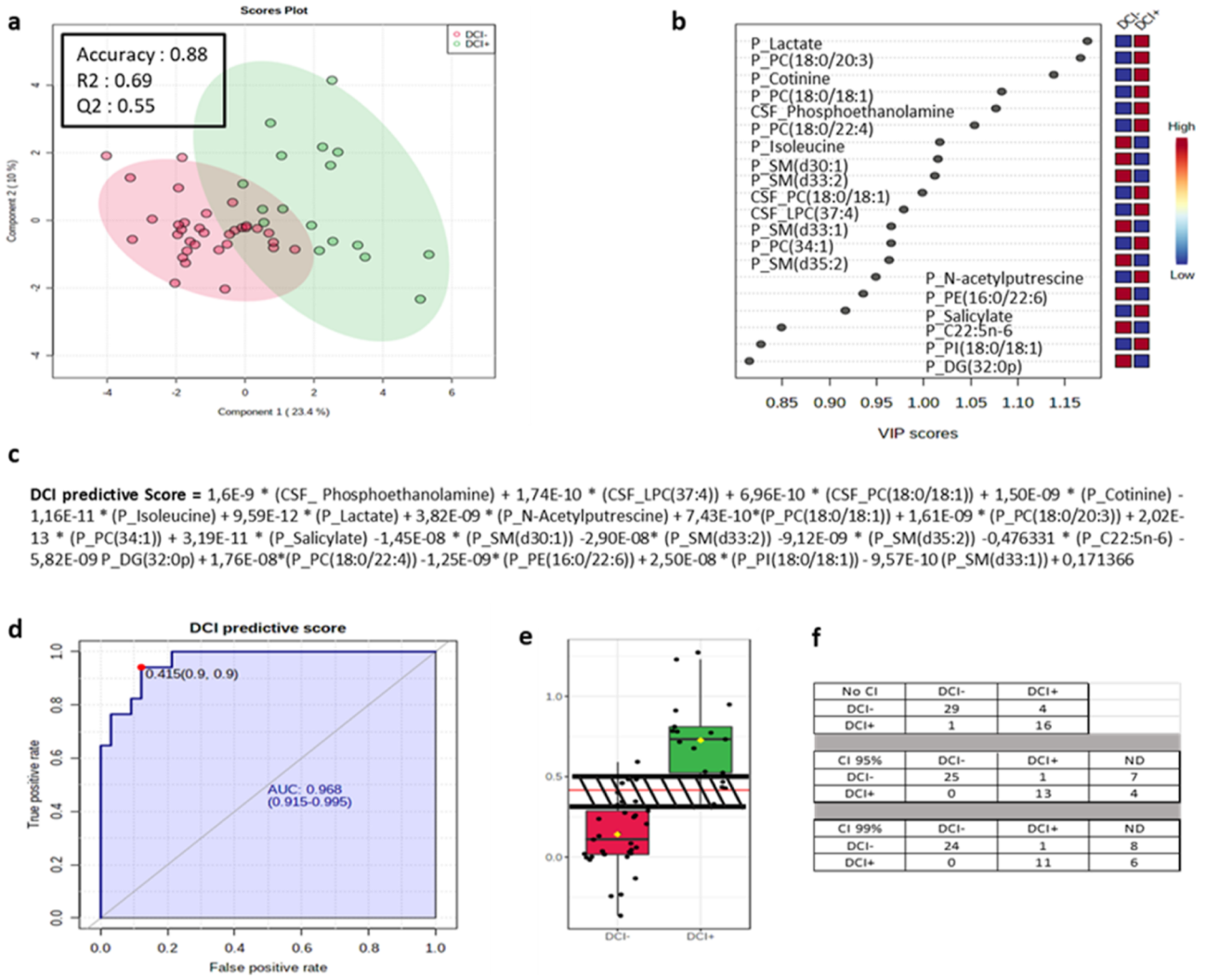

Figure 1. DCI predictive score and biomarker analysis. (a) PLS-DA 2D score plot showing the distribution of DCI+ and DCI− patients according to principal components 1 and 2. (b) VIP scores plot of the 20 metabolites selected in the final PLS-DA model. P and CSF prefixes for metabolite names indicate that the corresponding metabolites were detected in plasma and cerebrospinal fluid, respectively. (c) Equation of the composite score for prediction of the DCI status. P and CSF prefixes indicate if the corresponding metabolites are detected in plasma or CSF. (d) Receiver operating characteristic curve associated with the DCI predictive score. The red point represents the best cutoff according to sensitivity and specificity. AUC: area under the curve. (e) DCI predictive scores plot. The red line represents the test cutoff (0.415). The shaded area represents the 95% confidence interval (CI) gray zone. (f): DCI status prediction according to the DCI predictive score when applying no CI, 95% CI, and 99% CI. ND: not determined. The number of patients in each observed DCI status group is given in the corresponding rows. The number of patients in each predicted DCI status group is given in corresponding columns. Lipids key: DG, diacylclycerol; LPC, lysophosphatidylcholine; PC, phosphatidylcholine; PE, phosphatidylethanolamine; PI, phosphatidylinositol; and SM, sphingomyelin. The fatty acids esterified into complex lipids are indicated either individually with their carbon and insaturation numbers or together by the total number of carbon and insaturation in the corresponding lipid species when no distinction is possible. "d" stands for an amine ester, and "p" stands for an ether-linked lipid.

The selected metabolites were subsequently combined to generate a meaningful clinical composite score for each individual. This predictive score was calculated from the PLS algorithm using the PLS partial correlation coefficients applied to each metabolite, with the DCI status used as the predicted variable (Figure 1c). Working from this equation, we calculated a predictive DCI score for each individual and tested each score using a receiver operating characteristic curve (Figure 1d). The area under the curve was 0.968, the specificity was 0.88, the sensitivity was 0.94, and the cutoff threshold score above which DCI+ individuals were distinguished from DCI− ones was 0.415 (Figure 1d). When using the strict cut-off value, 86% (29/33) of aSAH patients without DCI and 94% (16/17) of aSAH patients with DCI were correctly assigned. Using a 99% CI and a 95% CI, 28% and 22%, respectively, were not defined, and no false-negative patients were found (Figure 1e,f). We validated our algorithm by also predicting the left-out patient samples from the 8 training sets described above. Only 6 out of the 48 excluded patients were classified in the wrong groups: 5 DCI+ and 1 DCI−. Of these 6 patients, three DCI + patients were not determined using 95% CI, and 2 DCI+ patients were correctly classified when considering the DCI score calculated for all patients. In addition, a retrospective power calculation indicated that 100% confidence at FDR of 0.05 can be achieved with a sample size of 17 patients per group, as was obtained in the DCI− group (seeFigure S3).

https://doi.org/10.1021/acs.jproteome.3c00575
J. Proteome Res. 2024, 23, 316−328

a

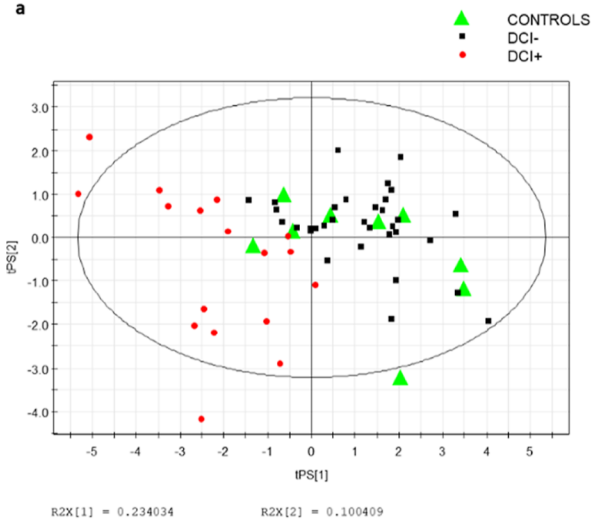

b

	Members	Correct	DCI-	DCI+	No class
DCI-	33	100%	33	0	0
DCI+	17	82.35%	3	14	0
CONTROLS	9		8	1	0
Total	59	94%	44	15	0
Fishers prob.	7.3e-010				

c

Controls identification	Predicted class
C	DCI-
P	DCI-
P10	DCI-
P17	DCI-
P26	DCI-
P39	DCI+
P42	DCI-
P52	DCI-
P56	DCI-

Figure 2. Predictive performance of the multiplex biomarker on control patients with no diagnosed aSAH (a) DCI+ (red dots) and DCI− (black squares) are used as a PLS-DA training model to visualize control patients with no aSAH and no DCI using the multiplex biomarker. (b) confusion matrix and class assignment probability calculated by the NIPALS algorithm from the PLS-DA model in panel (a). (c) class assignment of control patients calculated by the ROC.

Table 2. Pairwise Partial Correlation Network Characteristics Calculated in Either DCI+ (n = 17) or DCI− (n = 33) Patients

network characteristics	DCI− patients	DCI + patients	common pairwise correlations
correlation P value cutoff to obtain similar network density	0.0048	0.01	
network density (number of edges/nodes)	6.81 (5276/772)	6.83 (5605/823)	2.8% (295)
% of variables in network	91.5%	97.5%	
% of inter-CSF and plasma metabolite[a] correlations	30.35 (1701)	33.17%	0.1% (5)
% of intra-CSF + intraplasma metabolite correlations	69.65% (3575)	66.83% (3854)	1.1% (81)
% of total metabolites involved in the inter-CSF/plasma correlations	71.5%	68.5%	
% of total metabolites involved in the intra-CSF or intraplasma correlations	88,7%	96.5%	
% of common metabolites involved in both intra and inter-CSF/plasma correlations	77.2%	75.3%	
number of metabolites involved in the plasma and CSF cotinine, salicylate, and lactate subnetworks (Figures S8 andS9)	137	86	

[a]Generic term for both metabolites and lipids.

Finally, the predictive algorithm was challenged against control patients who had been admitted to the NCCU but were diagnosed with other neurological disorders (seeTable S1). Our model correctly classified all (but one) of these patients as DCI−, as expected (Figure 2).

Interplay between the Metabolome and Lipidome of Plasma and CSF

In an endeavor to delve deeper into the intricate relationships between the plasma and CSF metabolome and lipidome, we constructed a comprehensive pairwise correlation network between metabolites and lipids within DCI+ or DCI− patient groups. To mitigate potential biases stemming from variations in patient numbers between the groups, we generated networks with a comparable density (number of edges per node) (see Table 2). Notably, in both DCI+ and DCI− patients, approximately one-third of the total network correlations specifically delineated associations between plasma and CSF metabolites (refer to Table 2). These correlations encompassed approximately 72−75% of all analyzed metabolites/lipids in both biofluids (see Table 2). In contrast, there were only a minimal number of common correlations observed between DCI+ and DCI− patients (Table 2).

Multiblock Analysis

Annotated metabolites detected in CSF and plasma were clustered into 47 and 81 functional biological blocks, respectively, as described in Method Section[6,18] (see Tables S2 and S3). Lipids were blocked according to statistical proximity using hierarchical clustering analysis into 14 and 15 different blocks for CSF and plasma, respectively[6,18] (see Figure S4 and Tables S4 and S5). Notably, whereas the overlap between CSF and plasma metabolites was 31.9% (Figure S2), the corresponding overlap was 79.2% when grouping the metabolites into metabolic functions (Figure S5).

Each functional block was then analyzed using a hierarchical PLS-based approach (hierarchical PLS) on the entire cohort (n = 61). We tested the effectiveness of the blocking procedure to ensure it did not distort the mapping of observations in the PLS space by comparing the PLS-DA score plots of the

https://doi.org/10.1021/acs.jproteome.3c00575
J. Proteome Res. 2024, 23, 316−328

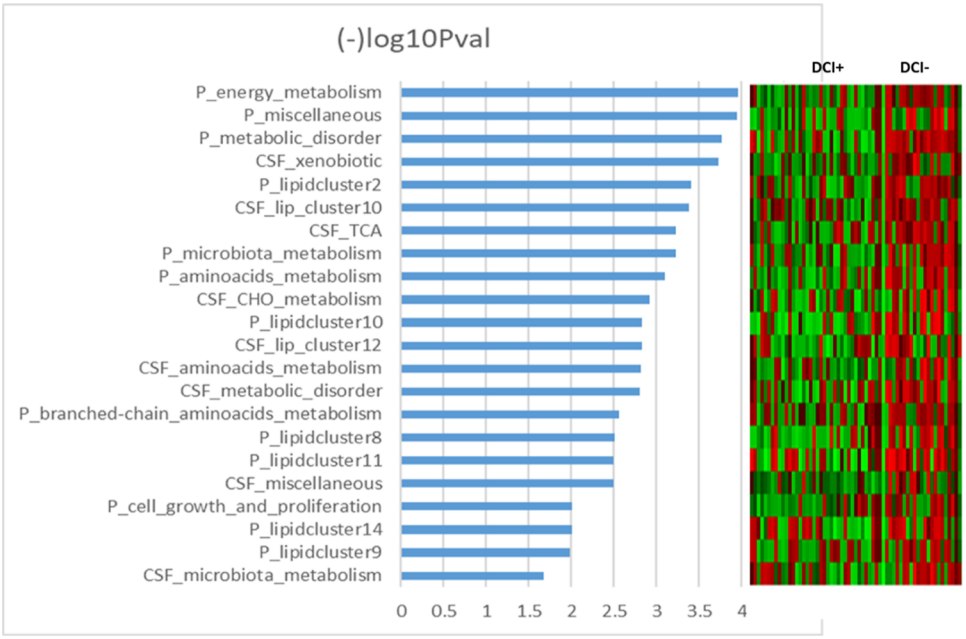

Figure 3. Influence of each metabolic function and lipid cluster in determining DCI status from analyses performed at t0 (first 24 h post-aSAH). The variables are sorted according to their *p*-value after −log10 transformation (where low *p*-values indicating high significance correspond to high log-transformed values). The right inset shows the heatmap score values of the corresponding functions and clusters for each patient. See Tables S2 and S3 for full details on metabolic function and lipid cluster compositions.

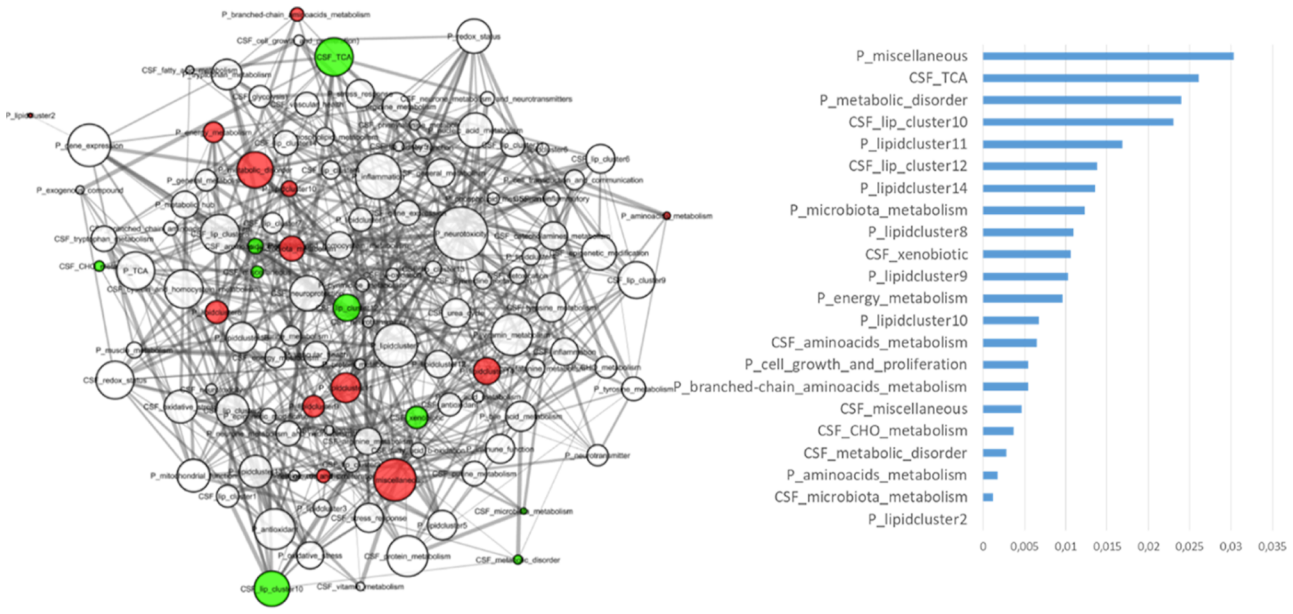

Figure 4. Minimum pairwise partial correlation network integrating all the metabolic functions and lipid clusters in future DCI+ patients and cleaned up from the edges of DCI− patients. The significant functions and clusters of Figure 3 are mapped in the network, with red nodes for plasma and green nodes for cerebrospinal fluid. Edge size is proportional to the *p*-value of the pairwise relationships. Node size relates to the value of the difference centrality coefficients calculated in Cytoscape. These coefficients used for the selection of the 22 significant nodes are also reported in decreasing order in the right inset. The detailed node composition, along with the betweenness centrality coefficients and *P* values, are reported in Table S6.

weighted block against the original unblocked data[6,18] (see Figure S6).

Using a statistical multitest procedure, we found a set of 14 biological functions and 8 lipid clusters in both plasma and CSF that were differentially regulated between DCI+ and DCI− patients (see Figure S7).

We then set out to hierarchize metabolic functions and lipid clusters that had the most impact on predicting the DCI phenotype. For that purpose, we first arbitrarily used the *t*-test *p*-values of the 14 biological functions and 8 lipid clusters previously selected (Figure 3).

Given that the metabolic regulations rarely occurred independently,[21] we calculated a pairwise partial correlation network integrating all the functions and clusters connected within and between plasma and CSF in future DCI+ patients (Figure 4). This allowed one to highlight nodes with important

https://doi.org/10.1021/acs.jproteome.3c00575
J. Proteome Res. 2024, 23, 316−328

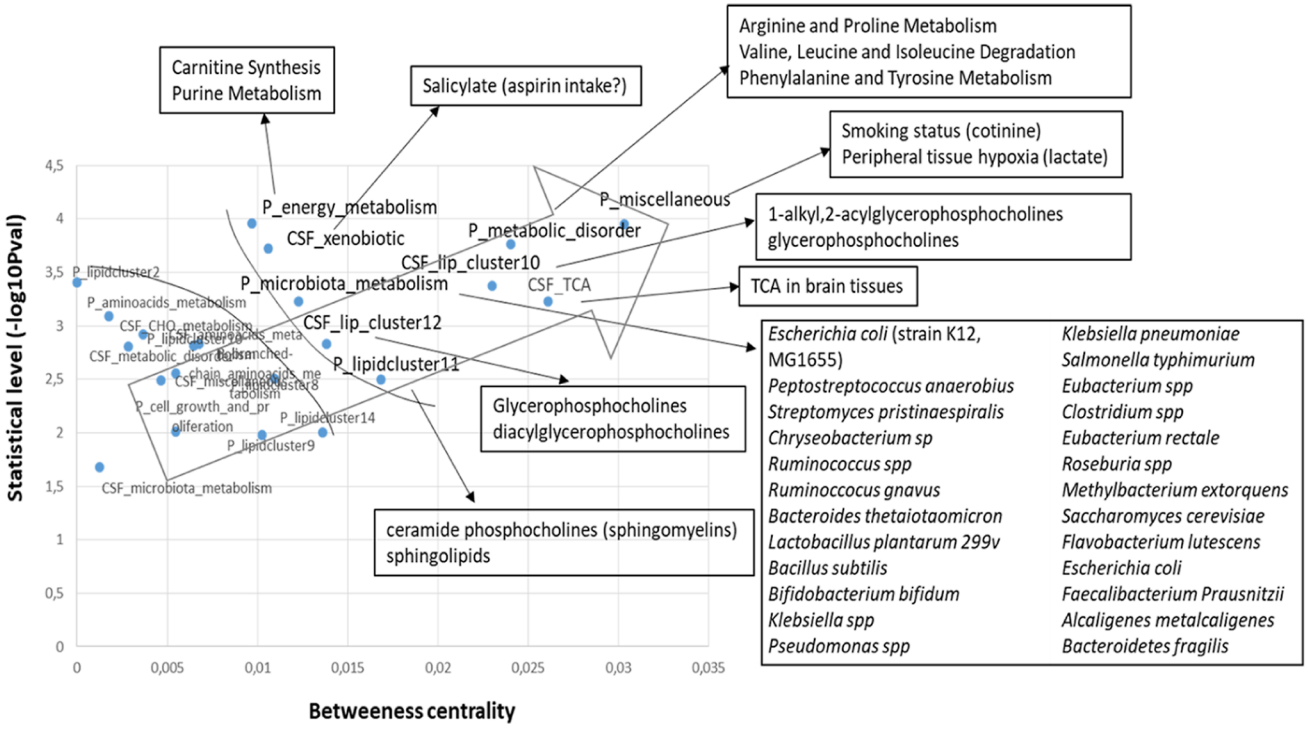

Figure 5. Betweenness centrality plotted against statistical *t*-test *p*-value for the 22 selected metabolic functions and lipid clusters. The most relevant variables for both the *P*-value and betweenness centrality coefficient are highlighted in the upper-right region of the plot. The empty arrow serves to further rank the relevance of each function in DCI occurrences. Functions aligned with the arrow direction are deemed increasingly important. The individual components of each function and cluster are further analyzed using the enrichment tool to translate the functions into molecular regulation. When enrichment was not appropriate (CSF_xenobiotics and P_miscellaneous), the main individual variable driver was reported. The putative bacteria producing metabolites of the P_microbiota metabolism function are reported. Links between metabolites and gut bacteria are indicated in Table S7.

connectivity by calculating the coefficient of betweenness centrality, which represents the degree to which nodes stand between each other. A node with higher betweenness centrality would have more control over the network and, thus, over the metabolic systems. Thus, besides the statistical significance, this dimension of the network topology also affords a way to gauge how far specific metabolic regulations influence a biological system.[22]

Finally, we plotted the distance centrality coefficient (Figure 4) with the corresponding *p*-value (Figure 3) of each cluster and function. This allows us to highlight the regulations that most influence the metabolic systems related to the development of DCI (Figure 5).

Based on this dual filtering analysis (*P* value and betweenness centrality), the miscellaneous score value appeared to have greater importance for determining patient DCI status. The miscellaneous cluster gathers all metabolites that are not frequent enough to constitute a functional set (at least 3 metabolites per set). The miscellaneous score was mainly driven by both higher plasma cotinine and higher plasma lactate in DCI+ patients (Figures 5 and S8).

The metabolic disorder function, comprising 32 metabolites, was associated with dysregulation of important metabolic pathways such as arginine and proline metabolism, branched-chain amino acid availability, and tyrosine and phenylalanine metabolism. Energy metabolism (comprising 8 metabolites) also emerged as important and mainly had impacts on carnitine synthesis and purine metabolism. Also, a part of sphingolipid metabolism appeared to be associated with further DCI occurrence in aSAH patients.

We also found that the microbiota metabolism score calculated from 18 plasma metabolites differed according to DCI status. These metabolites can be produced by 23 different bacterial species (Table S7), whose metabolism possibly varies according to patient DCI status. We also found functions in CSF that were relevantly associated with the further clinical outcome but that were different from those found in plasma. Tricarboxylic acid cycle regulation appeared different between the two patient outcomes, as did two lipid clusters related to ether lipids and glycerophosphocholine lipid species. Note that a cluster comprising xenobiotics in CSF scored differently according to patient DCI status and was mainly driven by higher CSF salicylate in DCI+ patients.

When focusing on specific metabolites, such as cotinine, salicylate, and lactate, previously implicated in DCI modulation (as indicated above and in Figure 5), they exhibited distinct correlation patterns between plasma and CSF, as illustrated in Figures S8 and S9. While these metabolites were interconnected within a metabolite cluster, their links between plasma and CSF displayed a more straightforward pattern in DCI+ patients compared to DCI− patients. Additionally, the two subnetworks involving cotinine, salicylate, and lactate exhibited divergent characteristics based on the patients' future outcomes (see Table 2).

DISCUSSION

DCI is one of the worst complications of aSAH but also one of the most common: it occurs in approximately 30% of patients, usually between postbleed day 5 and 14, and is associated with poor outcomes.[23] DCI has a highly complex set of underlying

https://doi.org/10.1021/acs.jproteome.3c00575
J. Proteome Res. 2024, 23, 316−328

mechanisms that include cerebral vascular dysfunction, microthrombosis, cortical spreading depolarization, and neuroinflammation.[3]

Identifying early predictive biomarkers of DCI at hospital admission would mark a huge step forward for managing aSAH patients in neurological critical care. A deeper understanding of the biological dysregulations associated with DCI could lead to novel therapeutic strategies.

To address these challenges, this study had two main goals: (i) to identify a shortlist of predictive biomarkers of DCI in patients admitted to the NCCU with spontaneous aSAH in blood and CSF sampled in the first 24 h post-aSAH; (ii) to identify early metabolic deregulations that lead to this life-threatening complication. To the best of our knowledge, this study is the first to report the results of metabolomics and lipidomics approaches on both plasma and CSF in patients with aSAH.

We identified a set of 20 metabolites from both plasma and CSF that are putative predictive biomarkers of DCI. These metabolites were combined into an equation that generated a per-patient score that was sufficiently sensitive and selective (0.94 and 0.88, respectively) (Figure 1). We also found that a 100% confidence at FDR of 0.05 can be achieved with a sample size of 17 patients per group, as was obtained in the DCI− group following a retrospective power calculation (see Figure S3). This kind of strategy has proven valuable in other studies for defining a biomarker that is less affected by interindividual variation or uncontrolled environmental influences.[18] The multiplex biomarker score at the 99% CI was not associated with false-negative results and can therefore identify patients who are not at risk for developing DCI (Figure 1). It is of interest that independent control patients with neither aSAH nor DCI were quite confidently assigned as no-DCI cases, as expected. This substantially consolidates the relevance of our metabolite panel and score for improving the DCI prognosis. Furthermore, our new multiplex biomarker shows better performance than the sole MMP-9 biomarker we previously used.[15] This important key step raises prospects for replicating our findings in a multicentric study and for precisely quantifying each selected metabolite to generalize the results.

This panel of 20 metabolites is composed of 14 lipids and 6 polar metabolites. Here, we found that blood lactate has the greatest discriminant power in the panel of metabolites. Nevertheless, other studies have yielded inconsistent results for blood lactate: like here, some showed that blood lactate correlates to aSAH outcomes,[12,24] whereas others did not.[25] This highlights the risk of using a single biomarker approach to predict the DCI, as it can be influenced by orthogonal events.

Cigarette smoking is one of the biggest risk factors for aSAH[26−29] and for recurrent aSAH after aneurysm repair,[29] and it has also been associated with symptomatic vasospasm after aSAH.[30,31] Our results are consistent with these findings, as vasospasm is one of the factors contributing to DCI pathophysiology, and 90.1% of the DCI+ patients in our study experienced a vasospasm. Cotinine is a nicotine metabolite that is widely used as a biomarker of cigarette smoking. Here, we found a higher level of cotinine in DCI+ patients, whereas the reported smoking status appeared to be less obvious (Table 1). This could be due to underreporting by patients or passive smoking.

The reduced set of 20 metabolites identified through this biomarker approach remains insufficient to provide a mechanistic explanation for complex disease phenotypes. Therefore, in order to push forward and decipher the metabolic dysregulations associated with DCI, we employed multiblock analysis and enrichment analysis that together make it possible to summarize complex metabolite profiles into meaningful functions or pathways as well as to plot the relationships of each set of functions and clusters in an interaction network. In this context, while the intersection of the two biofluids may seem limited when considering individual metabolites (approximately 32%, as illustrated in Figure S2), this heterogeneity dissipates when examining the broader scope of metabolic functions. This broader perspective aligns with the convergence of macroscopic regulations governing all cells and tissues, as depicted in Figure S5.

Then, crossing the statistical impact of the functions/clusters with the interaction network topology helped to hierarchize the impact of each biological module on future DCI occurrences (Figure 5). For instance, the "miscellaneous" cluster of metabolites had the best statistical power associated with the influence of the metabolic system (betweenness centrality) in defining DCI status. Since this cluster was mainly driven by plasma cotinine and plasma lactate, it again highlights the major influence of early peripheral tissue hypoxia together with smoking status for predicting a poor-prognosis DCI event, as observed elsewhere.[12]

Note that the xenobiotic cluster in CSF was significantly predictive of further DCI status, and much of this predictive power was driven by higher CSF salicylate concentrations in DCI+ patients. Plasma salicylate likely arose from aspirin intake and its subsequent deacetylation,[32] which would be higher in DCI + patients and may well represent a surrogate marker of the frequency of headache at aSAH onset. It could be important to monitor aspirin intake and the underlying reasons for aspirin use in adolescent aSAH patients. Significantly, upon scrutinizing the correlative relationships among the pivotal DCI-associated metabolites mentioned above—salicylate, cotinine, and lactate—it is evident that they consistently manifest within a tightly knit coregulation complex cluster in both plasma and CSF (Figures S9 and S10). This clustering underscores their collective significance in contributing to the direct or indirect etiology of DCI.

Enrichment analysis of lipid species in specific relevant lipid clusters pointed to a lower level of some subspecies of sphingomyelins in plasma and a higher level of some phosphatidylcholine subspecies and derivatives in both plasma and CSF in DCI+ patients (Figures S11 and S12). It is not possible at this stage to establish whether a metabolic deregulation of a specific lipid directly drives DCI or is merely a surrogate mechanism. However, as sphingomyelins are metabolized in ceramides (CER) by sphingomyelinase (SMase), a lower level of sphingomyelins could be a consequence of higher SMase activity. Testai et al.[8] found an elevated level of ceramides, particularly C18:0, within 48 h postbleed in the CSF of patients with symptomatic vasospasm. CER are important mediators of apoptosis, and several studies have described increased CER levels in stroke patients.[33] Moreover, SMase-driven CER production induces IL-6 expression[8,34] and triggers the vasoconstrictive properties of sphingolipids.[35,36] Further studies are needed to determine whether lower plasma levels of specific sphingomyelins in DCI + patients are linked to enhanced ceramide production and the occurrence of vasospasm.

The metabolites in three biological functions, namely, metabolic disorders and energy metabolism in plasma and

https://doi.org/10.1021/acs.jproteome.3c00575
J. Proteome Res. 2024, 23, 316−328

the tricarboxylic acid cycle (TCA) in CSF, can be translated into metabolic pathways using enrichment analysis. These functions are related specifically to arginine and proline metabolism, phenylalanine and tyrosine metabolism, branched-chain amino-acid degradation, carnitine synthesis, and purine metabolism. Greater TCA cycle deregulation in the brain might well be related to the hypoxia described by high plasma lactate levels, reflecting a greater global impairment of aerobic respiration, with mitochondria as the main target.[37] This global impairment might also be related to the difference in energy metabolism attached to carnitine and purine metabolism and measured in plasma between the future DCI + and DCI− cases. Other impairments also applied to the metabolic deregulations observed in plasma that were related to arginine and proline, phenylalanine and tyrosine, and branched-chain amino-acid metabolisms. NO bioavailability is central to controlling brain perfusion in DCI[38] and is related to arginine metabolism. Phenylalanine and tyrosine metabolism are related to catecholamine synthesis, and high plasma catecholamine levels were found to be related to poor aSAH outcomes.[38] Our observation further highlights the relationships between aSAH-catecholamine-mediated stress and high circulating lactate, as hypothesized by Van Donkelaar et al.[12] Note that rat studies have found a relationship between aberrant branched-chain amino acid metabolism and ischemic stroke. This relationship was due to dysregulation of the microbiota−gut−brain axis.[39] No such mechanism associating BCAA and microbiota has yet been reported for aSAH and DCI, but our finding that the BCAA metabolism is linked to the microbiota metabolism, potentially involving bacterial species, is consistent with.[39] Most previous studies on aSAH and consecutive DCI have focused on brain metabolic issues. Most of them, except for Van Donkelaar et al.[12] have largely ignored the relationship of brain metabolic impairments with peripheral metabolism. It is established that such a relationship greatly influences the incidence and severity of ischemic stroke and can impact postischemic stroke outcome.[40] Our results in aSAH patients also pointed to such interaction and integration between systemic and cerebral metabolism, as touched on elsewhere.[12] How this peripheral impairment would affect DCI occurrence remains unknown. It could also be a reflection in the plasma of metabolic deregulation in the brain following disruption of the blood−brain barrier[37] and could be specific to a poor DCI outcome. Similar to traumatic brain injuries (TBI), aneurysmal subarachnoid hemorrhage (aSAH) involves neuroinflammation.[3,41,42] This condition frequently induces substantial peripheral pathophysiological changes, yielding bidirectional consequences that influence diverse organ systems. These effects encompass the autonomic nervous system and the systemic inflammatory response, impacting vital organs, including the heart, lungs, gastrointestinal tract, liver, kidneys, spleen, and bones.[41,42] aSAH also features downstream complications, including respiratory distress,[43] which may contribute to the observed elevation in circulating lactate. The exploration of how initial peripheral hypoxia could, in turn, influence future DCI warrants further investigation. In addition, our findings reveal robust correlations between the metabolomes of CSF and plasma, evident not only at a macroscopic function level but also when scrutinizing individual metabolites (refer to Table 2 and Figures S9 and S10). Beyond individual contributing factors, this interconnectedness in the metabolomes of these two biofluids underscores further potential cerebroperipheral crosstalk in aSAH patients. Altogether, the above observations implied that addressing aSAH and further DCI may necessitate consideration of not only localized factors but also the induced early peripheral dysregulations.

The advantage of our multiblock approach is that it is possible to hierarchize the importance of each of the above-discussed events and metabolic deregulations associated with DCI outcomes, as illustrated in Figure 5. This hierarchization confirms that smoking status and systemic hypoxia are the main risk factors, followed by systemic metabolic deregulations likely associated with NO, catecholamine, and BCAA metabolism but also impairment of the tricarboxylic acid cycle in cerebral mitochondria and some phosphorylcholine lipids. Finally, other factors also emerged as slightly less important determinants of DCI, such as some aspects of peripheral sphingolipid metabolism and energy metabolism, gut microbes, and possibly also aspirin intake. Hence, following this ranking, targeting peripheral hypoxia could be a relevant strategy to help prevent DCI.

In conclusion, we identified a high-performance predictive metabolomic/lipidomic multiplex biomarker of future DCI in aSAH patients upon admission into neurological critical care. The integrative approach adopted here also highlighted important biological (both systemic and cerebral) deregulations associated with DCI occurrence, including peripheral hypoxia (blood lactate), specific lipid metabolism alterations, and deregulation of important metabolic functions. Analysis also pointed to possible exogenous causes of DCI, such as smoking and drug (aspirin) intake. Consequently, DCI not only manifests as a cerebral pathology but also extends to early peripheral deregulations. This discovery opens new avenues for potential treatment opportunities. Furthermore, our results importantly point for the first time to a possible gut microbiota−brain axis of DCI. However, the demonstration of such an influence would require dedicated protocols. The exploratory research reported here is based on a single-center study. This important first step was necessary to lay the foundations for a multicentric study to validate our results in different populations.

■ ASSOCIATED CONTENT

Data Availability Statement

For the availability of data and materials, the data sets generated during and/or analyzed during the current study are available from the corresponding author on reasonable request and within medical confidentiality restrictions.

Supporting Information

The Supporting Information is available free of charge at https://pubs.acs.org/doi/10.1021/acs.jproteome.3c00575.

Control patients used to test our predictive DCI score; biological function associated with metabolites in CSF; biological function associated with metabolites in plasma; composition of lipid blocks in CSF; composition of lipid blocks in plasma; betweenness centrality coefficients of a pairwise correlation network; links between gut bacteria and metabolites, according to published data; graphical summary of the clinical data before and after the normalization procedure; overlap of metabolites, lipid species, and total lipid fatty acids in CSF and plasma; predicted power according to sample size in each group using the 20 selected variables discriminating between DCI+ and DCI− patients;

https://doi.org/10.1021/acs.jproteome.3c00575
J. Proteome Res. 2024, 23, 316−328

clustering of the CSF and plasma lipidomes of the study population for hierarchical PLS analysis; overlap of the metabolic functions formed from the metabolites detected in both cerebrospinal fluid (CSF) and plasma; model performance in unblocked (left panel) and blocked (right panel) PLS-DA models; Venn plot showing the most common biological functions and lipid clusters that were shown to be significant using either the univariate *t*-test (with FDR-adjusted *p*-value at 0.05), the machine-learning random forest variable importance values, or PLS-DA VIP values; mass spectrometry detector response values for plasma cotinine and plasma lactate in DCI+ and DCI− patients; partial correlation subnetwork of plasma and CSF salicylate, cotinine, and plasma lactate in DCI+ patients; partial correlation subnetwork of plasma and CSF salicylate, cotinine, and plasma lactate in DCI− patients; lipid composition of plasma lipid cluster 11 with top discriminating lipid species (random forest variable importance index, as mean decrease accuracy); and lipid composition of plasma lipid cluster 10 and 12 with top discriminating lipid species (random forest variable importance index, as mean decrease accuracy) (PDF)

AUTHOR INFORMATION

Corresponding Author

Jean-Charles Martin − *Centre Cardiovasculaire et Nutrition (C2VN), INRAE, INSERM, Aix Marseille Université, Marseille 13005, France;* orcid.org/0000-0002-2870-0012; Email: jean-charles.martin@univ-amu.fr

Authors

Karim Chikh − *Service de Biochimie et Biologie Moléculaire, Hôpital Lyon Sud, Hospices Civils de Lyon, Pierre-Bénite 69310, France; Laboratoire CarMeN, Inserm U1060, INRAE U1397, Université de Lyon, Université Claude-Bernard Lyon1, Pierre-Bénite 69310, France;* orcid.org/0000-0002-1217-4193

David Tonon − *Centre Cardiovasculaire et Nutrition (C2VN), INRAE, INSERM, Aix Marseille Université, Marseille 13005, France; Service d'Anesthésie et Réanimation, Hôpital de La Timone, Marseille 13005, France*

Thibaut Triglia − *Centre Cardiovasculaire et Nutrition (C2VN), INRAE, INSERM, Aix Marseille Université, Marseille 13005, France; Service d'Anesthésie et Réanimation, Hôpital de La Timone, Marseille 13005, France*

David Lagier − *Centre Cardiovasculaire et Nutrition (C2VN), INRAE, INSERM, Aix Marseille Université, Marseille 13005, France; Service d'Anesthésie et Réanimation, Hôpital de La Timone, Marseille 13005, France*

Anouk Buisson − *Service de Biochimie et Biologie Moléculaire, Hôpital Lyon Sud, Hospices Civils de Lyon, Pierre-Bénite 69310, France*

Marie-Christine Alessi − *Centre Cardiovasculaire et Nutrition (C2VN), INRAE, INSERM, Aix Marseille Université, Marseille 13005, France*

Catherine Defoort − *Centre Cardiovasculaire et Nutrition (C2VN), INRAE, INSERM, Aix Marseille Université, Marseille 13005, France*

Sherazade Benatia − *Centre Cardiovasculaire et Nutrition (C2VN), INRAE, INSERM, Aix Marseille Université, Marseille 13005, France*

Lionel J. Velly − *Service d'Anesthésie et Réanimation, INT (Institut de Neurosciences de La Timone), Hôpital de La Timone, Aix Marseille Université, Marseille 13005, France*

Nicolas Bruder − *Service d'Anesthésie et Réanimation, Hôpital de La Timone, Marseille 13005, France*

Complete contact information is available at: https://pubs.acs.org/10.1021/acs.jproteome.3c00575

Author Contributions

L.V., N.B., M.C.A., J.C.M., T.T., and D.L. contributed to the study design. K.C., D.T., D.L., S.B., C.D., T.T., D.T., and D.L. participated in sample collection and analyses and clinical data registration. K.C. performed sample extraction, LC-MS/MS analysis, and bioinformatics processing. K.C. and J.C.M. performed statistical analyses and wrote the first draft of the manuscript. L.V., M.C.A., N.B., and C.D. revised the first draft. All authors read and approved the final version.

Funding

This work was partly supported by the Assistance Publique des Hôpitaux de Marseille (AORC project no. 2012-54).

Notes

The authors declare no competing financial interest.
For ethics approval for patients from the NCCU, informed consent was obtained according to local ethical guidelines. Ethical approval for this study (N8 2013-1316) was provided by the Ethical Committee of the Assistance Public Hôpitaux de Marseille, France (Chairperson Professor Jammes). The study was performed in accordance with the ethical standards laid down in the 1964 Declaration of Helsinki and its later amendments and conducted following the Strengthening the Reporting of Observational Studies in Epidemiology guidelines (STROBE).
Consent approval for publication is not applicable.
Clinical trial registration: Clinicaltrials.gov identifier: NCT02397759.

ACKNOWLEDGMENTS

Metaform (https://metaform-langues.fr/) provided professional English reviewing services.

LIST OF ABBREVIATIONS

aSAH, aneurysmal subarachnoid hemorrhage; BCAA, branched-chain amino-acids; CER, ceramides; CSF, cerebrospinal fluid; DCI, delayed cerebral ischemia; LC/MS, liquid-chromatography/mass spectrometry; PLS-DA, partial-least-squares discriminant analysis; SM, sphingomyelins; TCA, tricarboxylic acids; VIP, variable importance in projection

REFERENCES

(1) Diringer, M. N.; Bleck, T. P.; Claude Hemphill, J., III; Menon, D.; Shutter, L.; Vespa, P.; Bruder, N.; Connolly, E. S., Jr.; Citerio, G.; Gress, D.; et al. Critical care management of patients following aneurysmal subarachnoid hemorrhage: recommendations from the Neurocritical Care Society's Multidisciplinary Consensus Conference. *Neurocrit. Care* **2011**, *15* (2), 211−240. From NLM

(2) Vergouwen, M. D. I.; Ilodigwe, D.; Macdonald, R. L. Cerebral Infarction After Subarachnoid Hemorrhage Contributes to Poor Outcome by Vasospasm-Dependent and -Independent Effects. *Stroke* **2011**, *42* (4), 924−929.

(3) Geraghty, J. R.; Testai, F. D. Delayed Cerebral Ischemia after Subarachnoid Hemorrhage: Beyond Vasospasm and Towards a

Multifactorial Pathophysiology. *Curr. Atheroscler. Rep.* **2017**, *19* (12), 50. From NLM
(4) Milburn, M. V.; Lawton, K. A. Application of Metabolomics to Diagnosis of Insulin Resistance. *Annu. Rev. Med.* **2013**, *64* (1), 291−305.
(5) Cobb, J.; Gall, W.; Adam, K. P.; Nakhle, P.; Button, E.; Hathorn, J.; Lawton, K.; Milburn, M.; Perichon, R.; Mitchell, M.; et al. A novel fasting blood test for insulin resistance and prediabetes. *J. Diabetes Sci. Technol.* **2013**, *7* (1), 100−110.
(6) Fraser, K.; Roy, N. C.; Goumidi, L.; Verdu, A.; Suchon, P.; Leal-Valentim, F.; Tregouet, D. A.; Morange, P. E.; Martin, J. C. Plasma Biomarkers and Identification of Resilient Metabolic Disruptions in Patients With Venous Thromboembolism Using a Metabolic Systems Approach. *Arterioscler. Thromb. Vasc. Biol.* **2020**, *40* (10), 2527−2538.
(7) Alarcon-Barrera, J. C.; Kostidis, S.; Ondo-Mendez, A.; Giera, M. Recent advances in metabolomics analysis for early drug development. *Drug Discovery Today* **2022**, *27* (6), 1763−1773.
(8) Testai, F. D.; Hillmann, M.; Amin-Hanjani, S.; Gorshkova, I.; Berdyshev, E.; Gorelick, P. B.; Dawson, G. Changes in the Cerebrospinal Fluid Ceramide Profile After Subarachnoid Hemorrhage. *Stroke* **2012**, *43* (8), 2066−2070.
(9) Pilitsis, J. G.; Coplin, W. M.; O'Regan, M. H.; Wellwood, J. M.; Diaz, F. G.; Fairfax, M. R.; Michael, D. B.; Phillis, J. W. Free fatty acids in human cerebrospinal fluid following subarachnoid hemorrhage and their potential role in vasospasm: a preliminary observation. *J. Neurosurg.* **2002**, *97* (2), 272−279.
(10) Rostami, E.; Engquist, H.; Howells, T.; Johnson, U.; Ronne-Engström, E.; Nilsson, P.; Hillered, L.; Lewén, A.; Enblad, P. Early low cerebral blood flow and high cerebral lactate: prediction of delayed cerebral ischemia in subarachnoid hemorrhage. *J. Neurosurg.* **2018**, *128* (6), 1762−1770. From NLM
(11) Kofler, M.; Schiefecker, A.; Ferger, B.; Beer, R.; Sohm, F.; Broessner, G.; Hackl, W.; Rhomberg, P.; Lackner, P.; Pfausler, B.; et al. Cerebral Taurine Levels are Associated with Brain Edema and Delayed Cerebral Infarction in Patients with Aneurysmal Subarachnoid Hemorrhage. *Neurocrit. Care* **2015**, *23* (3), 321−329. From NLM
(12) van Donkelaar, C. E.; Dijkland, S. A.; van den Bergh, W. M.; Bakker, J.; Dippel, D. W.; Nijsten, M. W.; van der Jagt, M. Early Circulating Lactate and Glucose Levels After Aneurysmal Subarachnoid Hemorrhage Correlate With Poor Outcome and Delayed Cerebral Ischemia: A Two-Center Cohort Study. *Crit. Care Med.* **2016**, *44* (5), 966−972.
(13) Stapleton, C. J.; Acharjee, A.; Irvine, H. J.; Wolcott, Z. C.; Patel, A. B.; Kimberly, W. T. High-throughput metabolite profiling: identification of plasma taurine as a potential biomarker of functional outcome after aneurysmal subarachnoid hemorrhage. *J. Neurosurg.* **2019**, *133* (6), 1842−1849. From NLM
(14) Jabbarli, R.; Pierscianek, D.; Darkwah Oppong, M.; Sato, T.; Dammann, P.; Wrede, K. H.; Kaier, K.; Köhrmann, M.; Forsting, M.; Kleinschnitz, C.; et al. Laboratory biomarkers of delayed cerebral ischemia after subarachnoid hemorrhage: a systematic review. *Neurosurg. Rev.* **2020**, *43* (3), 825−833.
(15) Triglia, T.; Mezzapesa, A.; Martin, J. C.; Verdier, M.; Lagier, D.; Dufour, H.; Bruder, N.; Alessi, M. C.; Velly, L. J. Early matrix metalloproteinase-9 concentration in the first 48 h after aneurysmal subarachnoid haemorrhage predicts delayed cerebral ischaemia: An observational study. *Eur. J. Anaesthesiol.* **2016**, *33* (9), 662−669. From NLM
(16) von Elm, E.; Altman, D. G.; Egger, M.; Pocock, S. J.; Gøtzsche, P. C.; Vandenbroucke, J. P. The Strengthening the Reporting of Observational Studies in Epidemiology (STROBE) statement: guidelines for reporting observational studies. *Lancet* **2007**, *370* (9596), 1453−1457. From NLM
(17) Vergouwen, M. D. I.; Vermeulen, M.; van Gijn, J.; Rinkel, G. J. E.; Wijdicks, E. F.; Muizelaar, J. P.; Mendelow, A. D.; Juvela, S.; Yonas, H.; Terbrugge, K. G.; Macdonald, R. L.; Diringer, M. N.; Broderick, J. P.; Dreier, J. P.; Roos, Y. B. Definition of delayed cerebral ischemia after aneurysmal subarachnoid hemorrhage as an outcome event in clinical trials and observational studies: proposal of a multidisciplinary research group. *Stroke* **2010**, *41* (10), 2391−2395. From NLM
(18) Martin, J. C.; Bal-Dit-Sollier, C.; Bard, J. M.; Lairon, D.; Bonneau, M.; Kang, C.; Cazaubiel, M.; Marmonier, C.; Leruyet, P.; Boyer, C.; et al. Deep phenotyping and biomarkers of various dairy fat intakes in an 8-week randomized clinical trial and 2-year swine study. *J. Nutr. Biochem.* **2023**, *113*, 109239. From NLM
(19) Aidoud, N.; Delplanque, B.; Baudry, C.; Garcia, C.; Moyon, A.; Balasse, L.; Guillet, B.; Antona, C.; Darmaun, D.; Fraser, K.; Ndiaye, S.; Leruyet, P.; Martin, J. C. A combination of lipidomics, MS imaging, and PET scan imaging reveals differences in cerebral activity in rat pups according to the lipid quality of infant formulas. *FASEB J.* **2018**, *32* (9), 4776−4790. From NLM
(20) Wold, S.; Kettaneh, N.; Tjessem, K. Hierarchical multiblock PLS and PC models for easier model interpretation and as an alternative to variable selection. *J. Chemom.* **1996**, *10* (5−6), 463−482.
(21) Oltvai, Z. N.; Barabasi, A. L. Life's Complexity Pyramid. *Science* **2002**, *298* (5594), 763−764.
(22) Frainay, C.; Jourdan, F. Computational methods to identify metabolic sub-networks based on metabolomic profiles. *Briefings Bioinf.* **2017**, *18* (1), 43−56. (acccessed 12/30/2022)
(23) van Gijn, J.; Kerr, R. S.; Rinkel, G. J. Subarachnoid haemorrhage. *Lancet* **2007**, *369* (9558), 306−318. From NLM
(24) Okazaki, T.; Hifumi, T.; Kawakita, K.; Shishido, H.; Ogawa, D.; Okauchi, M.; Shindo, A.; Kawanishi, M.; Inoue, S.; Tamiya, T.; et al. Serial blood lactate measurements and its prognostic significance in intensive care unit management of aneurysmal subarachnoid hemorrhage patients. *J. Crit. Care* **2017**, *41*, 229−233. From NLM
(a) Aisiku, I. P.; Chen, P. R.; Truong, H.; Monsivais, D. R.; Edlow, J. Admission serum lactate predicts mortality in aneurysmal subarachnoid hemorrhage. *Am. J. Emerg. Med.* **2016**, *34* (4), 708−712. From NLM
(25) Poblete, R. A.; Cen, S. Y.; Zheng, L.; Emanuel, B. A. Serum Lactic Acid Following Aneurysmal Subarachnoid Hemorrhage Is a Marker of Disease Severity but Is Not Associated With Hospital Outcomes. *Front. Neurol.* **2018**, *9*, 593.
(26) Ballard, J.; Kreiter, K. T.; Claassen, J.; Kowalski, R. G.; Connolly, E. S.; Mayer, S. A. Risk factors for continued cigarette use after subarachnoid hemorrhage. *Stroke* **2003**, *34* (8), 1859−1863. From NLM
(27) Juvela, S.; Hillbom, M.; Numminen, H.; Koskinen, P. Cigarette smoking and alcohol consumption as risk factors for aneurysmal subarachnoid hemorrhage. *Stroke* **1993**, *24* (5), 639−646. From NLM
(28) Qureshi, A. I.; Sung, G. Y.; Suri, M. F.; Straw, R. N.; Guterman, L. R.; Hopkins, L. N. Factors associated with aneurysm size in patients with subarachnoid hemorrhage: effect of smoking and aneurysm location. *Neurosurgery* **2000**, *46* (1), 44−50. From NLM
(29) Koskinen, L. O.; Blomstedt, P. C. Smoking and non-smoking tobacco as risk factors in subarachnoid haemorrhage. *Acta Neurol. Scand.* **2006**, *114* (1), 33−37. From NLM
(30) Weir, B. K.; Kongable, G. L.; Kassell, N. F.; Schultz, J. R.; Truskowski, L. L.; Sigrest, A. Cigarette smoking as a cause of aneurysmal subarachnoid hemorrhage and risk for vasospasm: a report of the Cooperative Aneurysm Study. *J. Neurosurg.* **1998**, *89* (3), 405−411. From NLM
(31) Lasner, T. M.; Weil, R. J.; Riina, H. A.; King, J. T., Jr.; Zager, E. L.; Raps, E. C.; Flamm, E. S. Cigarette smoking-induced increase in the risk of symptomatic vasospasm after aneurysmal subarachnoid hemorrhage. *J. Neurosurg.* **1997**, *87* (3), 381−384. From NLM
(32) Dei Cas, M.; Rizzo, J.; Scavone, M.; Femia, E.; Podda, G. M.; Bossi, E.; Bignotto, M.; Caberlon, S.; Cattaneo, M.; Paroni, R. In-vitro and in-vivo metabolism of different aspirin formulations studied by a validated liquid chromatography tandem mass spectrometry method. *Sci. Rep.* **2021**, *11* (1), 10370.

https://doi.org/10.1021/acs.jproteome.3c00575
J. Proteome Res. 2024, 23, 316−328

(33) Kubota, M.; Kitahara, S.; Shimasaki, H.; Ueta, N. Accumulation of ceramide in ischemic human brain of an acute case of cerebral occlusion. *Jpn. J. Exp. Med.* **1989**, *59* (2), 59−64. From NLM
(34) Testai, F. D.; Xu, H. L.; Kilkus, J.; Suryadevara, V.; Gorshkova, I.; Berdyshev, E.; Pelligrino, D. A.; Dawson, G. Changes in the metabolism of sphingolipids after subarachnoid hemorrhage. *J. Neurosci. Res.* **2015**, *93* (5), 796−805. From NLM
(35) Altura, B. M.; Gebrewold, A.; Zheng, T.; Altura, B. T. Sphingomyelinase and ceramide analogs induce vasoconstriction and leukocyte-endothelial interactions in cerebral venules in the intact rat brain: Insight into mechanisms and possible relation to brain injury and stroke. *Brain Res. Bull.* **2002**, *58* (3), 271−278. From NLM
(36) Zheng, T.; Li, W.; Wang, J.; Altura, B. T.; Altura, B. M. Sphingomyelinase and ceramide analogs induce contraction and rises in [Ca(2+)](i) in canine cerebral vascular muscle. *Am. J. Physiol. Heart Circ. Physiol.* **2000**, *278* (5), H1421−H1428. From NLM
(37) Zhang, C.; Feng, L.; You, F.; Zhao, X.; Fang, X.; Zhou, Y. Whole-Brain Permeability Analysis on Admission Improves Prediction of Delayed Cerebral Ischemia Following Aneurysmal Subarachnoid Hemorrhage. *J. Stroke Cerebrovasc. Dis.* **2022**, *31* (4), 106312. From NLM
(38) Dodd, W. S.; Laurent, D.; Dumont, A. S.; Hasan, D. M.; Jabbour, P. M.; Starke, R. M.; Hosaka, K.; Polifka, A. J.; Hoh, B. L.; Chalouhi, N. Pathophysiology of Delayed Cerebral Ischemia After Subarachnoid Hemorrhage: A Review. *J. Am. Heart Assoc.* **2021**, *10* (15), No. e021845. From NLM
(39) Shen, J.; Guo, H.; Liu, S.; Jin, W.; Zhang, Z. W.; Zhang, Y.; Liu, K.; Mao, S.; Zhou, Z.; Xie, L.; et al. Aberrant branched-chain amino acid accumulation along the microbiota-gut-brain axis: Crucial targets affecting the occurrence and treatment of ischaemic stroke. *Br. J. Pharmacol.* **2023**, *180* (3), 347−368. From NLM
(40) Wesley, U. V.; Bhute, V. J.; Hatcher, J. F.; Palecek, S. P.; Dempsey, R. J. Local and systemic metabolic alterations in brain, plasma, and liver of rats in response to aging and ischemic stroke, as detected by nuclear magnetic resonance (NMR) spectroscopy. *Neurochem. Int.* **2019**, *127*, 113−124. From NLM
(41) Faden, A. I.; Barrett, J. P.; Stoica, B. A.; Henry, R. J. Bidirectional Brain-Systemic Interactions and Outcomes After TBI. *Trends Neurosci.* **2021**, *44* (5), 406−418. From NLM
(42) McDonald, S. J.; Sharkey, J. M.; Sun, M.; Kaukas, L. M.; Shultz, S. R.; Turner, R. J.; Leonard, A. V.; Brady, R. D.; Corrigan, F. Beyond the Brain: Peripheral Interactions after Traumatic Brain Injury. *J. Neurotrauma* **2020**, *37* (5), 770−781.
(43) Fan, T. H.; Huang, M.; Price, C.; Premraj, L.; Kannapadi, N. V.; Suarez, J. I.; Cho, S.-M. Prevalence and outcomes of acute respiratory distress syndrome in patients with aneurysmal subarachnoid hemorrhage: a systematic review and meta-analysis. *J. Neurocrit. Care* **2022**, *15* (1), 12−20.

https://doi.org/10.1021/acs.jproteome.3c00575
J. Proteome Res. 2024, 23, 316−328